JACS
JOURNAL OF THE AMERICAN CHEMICAL SOCIETY

Article

pubs.acs.org/JACS

A Molecular Ruthenium Electrocatalyst for the Reduction of Carbon Dioxide to CO and Formate

Charles W. Machan, Matthew D. Sampson, and Clifford P. Kubiak*

University of California—San Diego, Department of Chemistry and Biochemistry, 9500 Gilman Drive 0358, La Jolla, California 92023, United States

Supporting Information

ABSTRACT: The use of a bulky bipyridine ligand, 6,6′-dimesityl-2,2′-bipyridine (mesbpy), to enable the reduction of carbon dioxide by a Ru-based molecular electrocatalyst is reported. Under catalytic conditions, this compound exhibits turnover frequencies of 1300 s^{-1} and 95% Faradaic efficiency for the production of CO and H_2O from CO_2 in the presence of Brønsted acids. Mechanistic electrochemical and spectroelectrochemical studies, supplemented by the direct synthesis of relevant intermediates, indicate that this behavior is the result of the cooperative redox response of the bipyridine ligand and Ru metal center at negative potentials, as well as the inhibition of Ru−Ru bond formation through steric interactions.

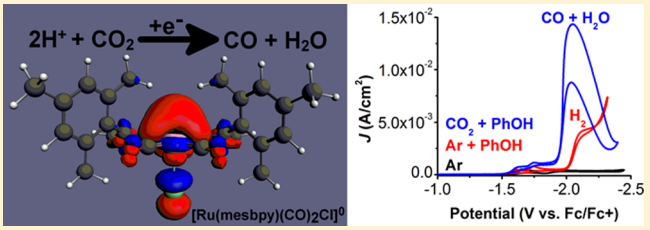

INTRODUCTION

The eventual depletion of petrochemical feedstocks and rising levels of carbon dioxide (CO_2) continue to drive interest in the use of CO_2 as a C_1 source for liquid fuels.[1−6] Electrocatalytic reduction offers a way to close the fuel cycle by using CO_2 in the synthesis of energy-dense molecules.[1,6] If done using renewable energy sources, this process could enable the storage of electrical energy in chemical bonds in an efficient and recoverable manner. Molecular catalysts have been shown to be active and selective for the electrocatalytic reduction of CO_2 to CO, but often have limited turnover frequencies (TOFs), high overpotentials, and poor stabilities. Recent progress has been made in benchmarking different catalysts for CO_2 reduction; however, this is still a work in progress.[7−10] To the limited extent to which the rates of molecular electrocatalysts can be compared, the "state-of-the-art" catalysts reported so far are Re and Mn(bpy)$(CO)_3$X (bpy = 2,2′-bipyridine, X = halide or a weakly coordinating anion), hydroxyphenyl-substituted Fe porphyrins, and Ni(cyclam)$^{2+}$ (cyclam = 1,4,8,11-tetraazacyclotetradecane).[10−14] Generally, molecular Ru-based electrocatalysts have shown much lower activities.[11,15,16] Under reducing conditions, complexes of the type Ru(bpy)$(CO)_2Cl_2$ have been shown to polymerize on the cathode through the formation of Ru−Ru bonds.[17−19] The resultant metallopolymer is highly active for the reduction of CO_2 to CO as a heterogeneous catalyst. Our group has shown that the use of a bulky bpy ligand, 6,6′-dimesityl-2,2′-bipyridine (**mesbpy**, **1**), inhibited metal−metal bond formation in the case of Mn tricarbonyl complexes, resulting in catalysts with TOFs in excess of 5000 s^{-1}.[13] Recently, Kuramochi et al. also reported that the use of the same bulky bpy ligand (**mesbpy**), instead of an unfunctionalized bpy ligand, for complexes of the type Ru(bpy)$(CO)_2Cl_2$ resulted in the selective photocatalytic production of CO from CO_2.[20] We reasoned that the use of the **mesbpy** ligand in the context of Ru-based molecular catalysts could have a similar effect on their electrocatalytic properties.

RESULTS

Metallating **mesbpy**[21] with the Ru(II) carbonyl precursor $[Ru(CO)_2Cl_2]_n$[22] (**2**) in refluxing toluene resulted in the isolation of *trans*-Cl-Ru(mesbpy)$(CO)_2Cl_2$ (**3**) as a pale yellow powder (Scheme 1).[20] X-ray crystallographic studies on single crystals grown from THF and pentanes show an octahedral coordination geometry around the Ru metal center, with the chloride ligands occupying axial positions, the bpy fully chelated in the equatorial plane, and two CO ligands at the remaining coordination sites (Figure 1, Table S1).[17,18,20] All other characterization data are consistent with this assignment. The plane of the bpy is slightly distorted: the N−C−C−N dihedral angle is 16.9(4)°.

Scheme 1. Synthesis of 3 from 1 and 2

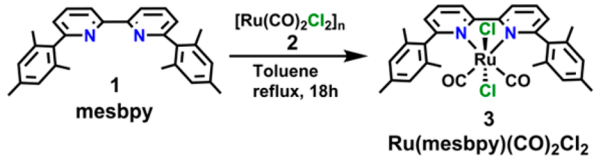

An initial electrochemical survey under Ar saturation showed two reduction features at negative potentials: the first at −1.69 V vs Fc/Fc+ is irreversible; the second at −1.86 V vs Fc/Fc+ is

Received: April 21, 2015
Published: June 18, 2015

DOI: 10.1021/jacs.5b03913
J. Am. Chem. Soc. 2015, 137, 8564−8571

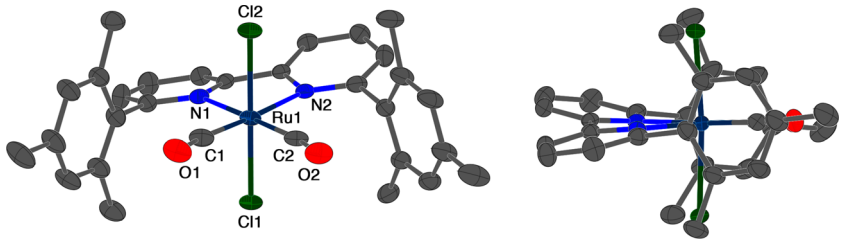

Figure 1. Molecular structure of **3** obtained from single-crystal X-ray diffraction studies; Ru = cerulean, C = gray, N = blue, Cl = green, O = red; thermal ellipsoids at 50%; H atoms omitted for clarity.

quasi-reversible (Figure 2, ΔE_p = 0.61 V; see Supporting Information). The current response of the first and second

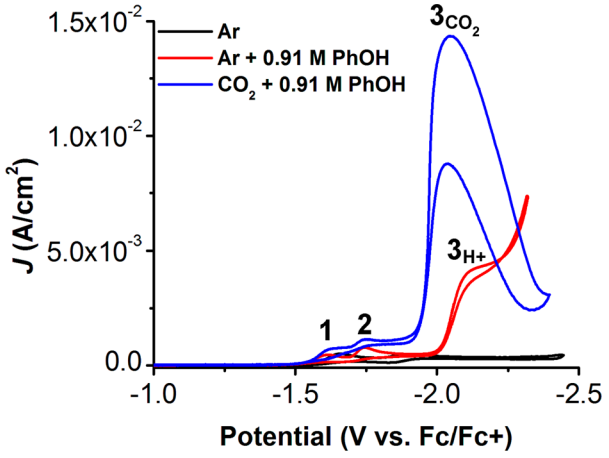

Figure 2. Cyclic voltammograms of **3** under Ar saturation (black), Ar saturation with added PhOH (red), and CO_2 saturation with added PhOH (blue). First, second, and third reduction waves labeled for clarity. Conditions: 1 mM **3**; 0.1 M $TBAPF_6$/MeCN; glassy carbon working electrode, Pt counter electrode, Ag/AgCl pseudoreference electrode; referenced to internal ferrocene standard; scan rate 100 mV/s.

reduction features show a dependence on scan rate consistent with a freely diffusing molecule (Figures S1, S2, and S3). Based on these observations, we assign the first reduction to a bpy-based reduction of **3** to $[Ru^{II}(mesbpy^{\bullet-})(CO)_2Cl_2]^-$, followed by Cl loss through a ligand-to-metal charge transfer (LMCT) to yield $[Ru(mesbpy)(CO)_2Cl]^0$, before a second bpy-based reduction to generate $[Ru^{I}(mesbpy^{\bullet-})(CO)_2Cl]^-$. The titration of phenol (PhOH) under Ar saturation revealed a new reduction feature (E_p = −2.12 V vs Fc/Fc+, $\mathbf{3}_{H+}$; Figures 2 and S4). The potential of the first reduction shows a dependence on PhOH concentration, which is indicative of a protonation step coupled to electron transfer (Figure S5).[13,23−25] The observed current response at the third reduction is consistent with second-order kinetic dependence on PhOH concentration (Figure S6). Bulk electrolysis experiments suggest that this new feature ($\mathbf{3}_{H+}$, Figure 2) represents the catalytic reduction of PhOH to H_2 (Table S2). No other gaseous products were detected by GC. Based on these observations, we assign the first feature (**1**, Figure 2) to an initial reduction followed by the formation of a cationic Ru−H, $[Ru^{III}(mesbpy)(H)(CO)_2Cl]^+$, through a protonation by PhOH. Using the concentration of added PhOH and the corresponding shift in potential, it is possible to determine a binding constant for H^+ by Ru of K_{H+} = 4.3 ± 1.4 M^{-1} under these conditions (Figure S5).[13,23−25] The subsequent reduction of this cationic species (**2**, Figure 2) is expected to generate $Ru^{II}(mesbpy)(H)(CO)_2Cl$. The third feature ($\mathbf{3}_{H+}$, Figure 2) corresponds to the reduction of $Ru^{II}(mesbpy)(H)(CO)_2Cl$ to generate a species, presumably $[Ru^{II}(mesbpy^{\bullet-})(H)(CO)_2Cl]^-$, which has sufficient hydricity to react with a proton and form H_2. We note that catalytic H_2 production from PhOH on glassy carbon electrodes does not occur until −2.60 V vs Fc/Fc+.[26]

Sparging the solution to saturation with CO_2 in the presence of added PhOH altered all three of these reduction features (Figure 2). Although reactivity was observed with CO_2 only, the adventitious addition of trace amounts of H_2O through CO_2 sparging precluded isolation of the pure CO_2 response (Figure S7). As was the case under Ar saturation, the first reduction wave showed a positive potential shift with titration of PhOH under fixed CO_2 concentration (∼0.28 M, Figure S8). The second reduction feature, however, did *not* shift as the concentration of added PhOH increased. Varying CO_2 concentration under a fixed concentration of PhOH (0.28 M) showed that only the *second* reduction potential was dependent on CO_2 concentration (Figure S9). Note that, in the presence of CO_2, the third reduction wave ($\mathbf{3}_{CO2}$, E_p = −2.05 V vs Fc/Fc +; Figure 2) is shifted >100 mV more positive than the feature in the presence of PhOH only ($\mathbf{3}_{H+}$) and there is a significant increase (∼3×) in the catalytic current density. The titration of PhOH under CO_2 saturation (∼0.28 M) also revealed that the current dependence of the third reduction feature was second-order in [PhOH] (Figures S10 and S11). Bulk electrolysis under CO_2 saturation with added PhOH confirmed that, at the third reduction (∼−2.2 V vs Fc/Fc+), this system was catalytic, showing 95% current efficiency for CO production through 5.2 turnovers (relative to moles of **3** in solution, Table S2). The formation of H_2 was negligible by GC (∼1%). When bulk electrolysis was repeated at the second reduction potential (∼−1.7 V vs Fc/Fc+), the observed Faradaic efficiency for CO dropped to 63 ± 16% (H_2 accounted for 1.8 ± 0.8% of current passed under these conditions) and HCO_2H was observed by NMR (Figure S12). Insufficient current was observed at more positive potentials, precluding accurate product analysis. This indicates that the relative production of CO or HCO_2H is dependent on the applied potential. Similar effects on the ratio of CO to HCO_2H production have been observed for the Ru(bpy)-based metallopolymer when the applied potential was varied.[27] Similar to the results under Ar, these data are consistent with the assignment of the first feature to an initial reduction followed by a protonation by PhOH to form $[Ru^{III}(mesbpy)(H)(CO)_2Cl]^+$. The shift in potential at the first reduction feature when PhOH was varied approximates to a binding constant for H^+ by Ru of K_{H+} = 32 ± 9.2 M^{-1} (Figure S8).[23−25] A Pourbaix diagram generated from these data exhibits a slope of approximately 60 mV/pK_a unit of PhOH

DOI: 10.1021/jacs.5b03913
J. Am. Chem. Soc. 2015, 137, 8564−8571

under CO_2 saturation, which is also indicative of a $1e^-/1H^+$ process (Figure S13).[28−30] The increase in this binding constant under CO_2 from the value obtained under Ar is the result of a Nernstian shift from the favorable subsequent insertion of CO_2 into the Ru−H bond, *vide infra*. The second reduction is then expected to generate $Ru^{II}(mesbpy)(H)(CO)_2Cl$, which the data suggest undergoes a reaction with CO_2. The product of this reaction is expected to be a species similar to $Ru^{II}(mesbpy)(\eta^1\text{-}OCOH)(CO)_2Cl$.[31] A binding constant for CO_2 can be calculated from the change in potential at the second reduction under a fixed concentration of PhOH: K_{CO_2} = 28 ± 5.0 M^{-1} with 0.28 M PhOH (Figure S9). Based on a comparison of i_{cat}/i_p at the third reduction, which is proportional to the electrocatalytic rate constant and TOF, this catalyst is estimated to have a TOF for CO_2 reduction to CO of 1300 s^{-1} with 0.91 M PhOH (see Supporting Information for details).[13] The third reduction presumably corresponds to the reduction of $Ru^{II}(mesbpy)(\eta^1\text{-}OCOH)(CO)_2Cl$ to $[Ru^{II}(mesbpy^{\bullet-})(\eta^1\text{-}OCOH)(CO)_2Cl]^-$, which we did not expect to catalytically produce CO. In order to test these assignments more carefully, we explored the behavior of **3** further using spectroelectrochemistry.

Infrared spectroelectrochemistry (IR-SEC) experiments, which allow for characterization of changes in the IR signature with respect to potential and time, were used to investigate the behavior of **3** at negative potentials with and without substrate present.[32−34] At resting potentials under N_2 saturation, two IR bands are observed for **3** in $TBAPF_6$/MeCN at 2058 and 1995 cm^{-1} (Figure 3).[17,18,20] When the applied negative potential is

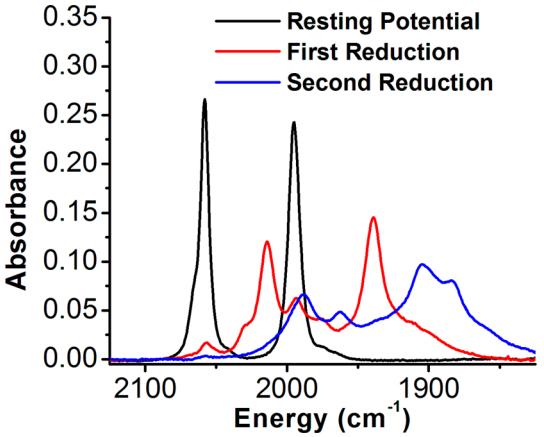

Figure 3. IR-SEC of **3** under N_2 saturation showing the species at resting potential (black), the first reduction (red), and the second reduction PhOH (blue). Conditions: 3.5 mM **3**; 0.1 M $TBAPF_6$/MeCN; Pt working electrode, Pt counter electrode, Ag pseudoreference electrode.

increased stepwise to the first reduction observed by CV (∼−1.5 V vs Fc/Fc+), these bands are replaced by two new bands at 2014 and 1939 cm^{-1} (with other minor species, *vide infra*). We assign this primary species to $[Ru(mesbpy)(CO)_2(MeCN)Cl]^0$, which results from a single-electron reduction, chloride loss from the parent species **3**, $Ru^{II}(mesbpy)(CO)_2Cl_2$, and MeCN solvent coordination. This assignment is consistent with the irreversible reduction observed by CV. The other minor bands observed at this potential likely correspond to two species: the six-coordinate anion, $[Ru^{II}(mesbpy^{\bullet-})(CO)_2Cl_2]^-$, which forms before Cl dissociation to form the major species, and the five-coordinate, neutral complex, $[Ru(mesbpy)(CO)_2Cl]^0$, which forms before solvent coordination. These assignments are supported by chemical reduction experiments with potassium-intercalated-graphite (KC_8, Figure S14). Other constitutional isomers, i.e. CO ligands at axial positions and solvent coordination in various positions, can occur upon losing the Cl ligand.[17−19,35−37] Increasing the applied negative potential again to that of the second reduction (∼−1.7 V vs Fc/Fc+) resulted in the appearance of two major bands at 1904 and 1884 cm^{-1}. These bands are consistent with a five-coordinate, anionic complex, $[Ru^{I}(mesbpy^{\bullet-})(CO)_2Cl]^-$ (see Figure S14 for more information on this assignment). The other minor bands observed at this second reduction potential could be results of the following: incomplete reduction to the doubly reduced complex, other isomers (as previously discussed), and MeCN solvent coordination.[35−37]

A second set of experiments with added PhOH (0.5 M) under N_2 saturation conditions indicated that at applied potential a reaction with PhOH was occurring. At resting potential, bands consistent with the starting material **3** were observed at 2058 and 1995 cm^{-1} (Figure S15). When the negative potential of the IR-SEC cell was increased stepwise to that of the first reduction observed by CV (∼−1.5 V vs Fc/Fc+), these bands diminished in intensity and were replaced by a species with absorbances at 2051 and 1984 cm^{-1}, with a minor species also observable at 2031 and 1960 cm^{-1}. The former is tentatively assigned to $[Ru^{III}(mesbpy)(H)(CO)_2Cl]^+$, *vide infra*, and the latter is assigned to $[Ru^{II}(mesbpy^{\bullet-})(CO)_2Cl_2]^-$ (Figure S14).[35,36] If the cell potential is increased again to more negative potentials corresponding to the second reduction (∼−1.7 V vs Fc/Fc+), the major species observable by IR becomes $Ru^{II}(mesbpy)(H)(CO)_2Cl$, with intense bands at 2029 and 1948 cm^{-1}, consistent with previous reports.[35,38] Although the shift in the observed carbonyl frequencies from 2051 and 1984 cm^{-1} to 2029 and 1948 cm^{-1} is not necessarily diagnostic of a change in oxidation state, it is clear from these experiments that the former is a product of a Ru^I reaction with H^+ and from literature precedent and direct synthesis that the latter represents a Ru^{II}−H species, *vide infra* (see Experimental Section).

When these experiments were repeated under CO_2 saturation with added PhOH (0.5 M), bands were observed which are consistent with the initial formation of a Ru−H species followed by rapid CO_2 insertion (Figure 4). At the first reduction potential (∼−1.5 V vs Fc/Fc+), two species are observed, with the first set of bands at 2050 and 1983 cm^{-1} and the second set of bands at 2032, 1958, and 1949 cm^{-1}. Over the course of 5 min the system equilibrates almost entirely to the second of these two species at this potential. Based on the previously described experiments, the former is tentatively assigned to $[Ru^{III}(mesbpy)(H)(CO)_2Cl]^+$ and the latter is assigned to $Ru^{II}(mesbpy)(\eta^1\text{-}OCHO)(CO)_2Cl$ (Figure S16).[31] We attribute the observation of products from an additional reduction at this potential to the Nernstian shift of the second reduction potential from the favorable binding of CO_2 by Ru^{II}−H. The region where Ru−(η^1-OCHO) adducts are expected (1500−1600 cm^{-1}) is obscured by the strong solvent absorbance.[39,40] At the second reduction potential (∼−1.7 V vs Fc/Fc+) new bands appear at 2016, 1989, 1945, and 1890 cm^{-1}, which are the only observable IR features at the second reduction potential and after the third reduction potential (∼−2.0 V vs Fc/Fc+, Figure 2). These species are likely

DOI: 10.1021/jacs.5b03913
J. Am. Chem. Soc. 2015, 137, 8564−8571

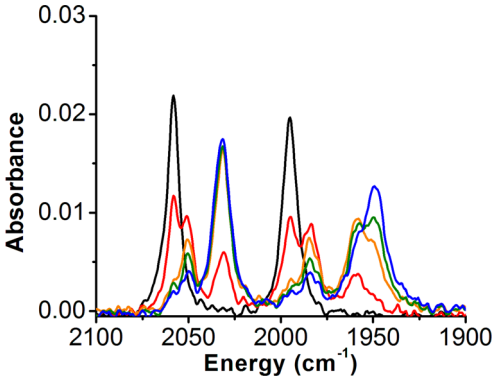

Figure 4. IR-SEC of **3** under CO_2 saturation with added PhOH (0.5 M) showing the species at resting potential (black) and those which grow in at the first reduction (red to blue) over the course of 5 min. Conditions: 8.6 mM **3**; 0.1 M $TBAPF_6$/MeCN; glassy carbon working electrode, Pt counter electrode, Ag pseudoreference electrode.

isomers of the type $[Ru^{II}(mesbpy^{\bullet-})(\eta^1\text{-OCOH})(CO)_2L]^X$ or $[Ru^{I}(mesbpy)(\eta^1\text{-OCOH})(CO)_2L]^X$, where L = MeCN or Cl (Figure S17).[35−37]

DISCUSSION

In general, the reduction of CO_2 proceeds by either a hydroxycarbonyl (***a***) or a HCO_2^- (***b***) bound intermediate (eq 1).

(1)

Mechanistic studies show that a hydroxycarbonyl complex is usually obtained by direct interaction of a reduced metal center with CO_2, followed by protonation.[41] A HCO_2^- adduct is usually produced by a metal hydride reacting with CO_2 to produce the C−H bond, followed by rearrangement to the O-bonded species, ***b***.[42,43] To our knowledge, there exists no detailed discussion concerning the potential isomerization between ***a*** and ***b***. The results described here suggest that the relative thermodynamic stabilities of ***a*** and ***b*** can depend on the redox states of the metal ions involved. Indeed, Ru(bpy) complexes have previously been reported to electrocatalytically or photocatalytically produce mixtures of HCO_2^-/HCO_2H and CO from CO_2 with varying efficiencies.[17,18,20,27,44−47] Our proposed reduction mechanism for the electrocatalytic process to HCO_2^- is shown in Scheme 2. The irreversibility of the observed CV response of **3** (***i***) at the first reduction is indicative of a bpy-based reduction followed by a fast ligand-to-metal charge transfer (LMCT) resulting in Cl loss, yielding $[Ru(mesbpy)(CO)_2Cl(L)]^0$ (***ii***). This interpretation of the reduction feature is also supported by DFT calculations, which suggest that the LUMO of ***i*** is localized on the π^* orbital of the bpy ligand (Figure S18). $[Ru(mesbpy)(CO)_2Cl(L)]^0$ reacts with H^+ to generate $[Ru^{III}(mesbpy)(H)(CO)_2Cl]^+$ (***iii***). Additional DFT calculations on the presumptive five-coordinate intermediate generated by L loss from ***ii***, $[Ru(mesbpy)(CO)_2Cl]^0$, indicate a cooperative metal−ligand redox response; the added charge in the SOMO is distributed between the d_{z^2} orbital of the metal center and the π^* orbital of the bpy ligand (Figure S19). Under applied potential under

Scheme 2. Proposed Overall Mechanism for the Reduction of CO_2 to CO and H_2O or HCO_2H by 3, Ar = Mesityl, L = MeCN

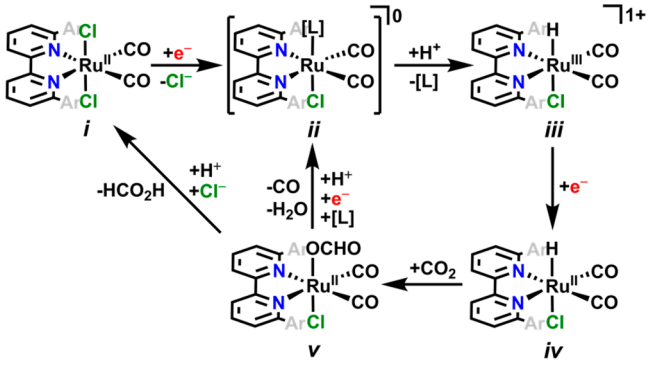

CO_2 saturation, however, this species is rapidly reduced to $Ru^{II}(mesbpy)(H)(CO)_2Cl$, ***iv***. An insertion reaction involving CO_2 and ***iv*** generates $Ru^{II}(mesbpy)(\eta^1\text{-OCHO})(CO)_2Cl$, ***v***. Bulk electrolysis at this potential shows that both CO and HCO_2^-/HCO_2H are generated. For CO production to occur, a dehydration reaction must take place involving the formato species: Ru complexes have previously been observed to catalyze the dehydration of HCO_2H.[22,48−50] Interestingly, the synthesis of the Ru(II) precursor used in these studies seems to rely on a similar mechanism to generate $[Ru(CO)_2Cl_2]_n$ from $RuCl_3$, HCl (aq.), and HCO_2H.[22]

If an additional reduction reaction involving ***v*** takes place, the dehydration reaction is accelerated, as evidenced by the increased current response for CO production observed at the third reduction feature by CV. Current efficiency for CO is almost quantitative at this potential, suggesting an efficient interconversion of HCO_2^- and H^+ to CO and H_2O. Generating CO from solvated HCO_2H is predicted to be favored over a decarboxylation reaction at room temperature as a result of the favorable solvation effects of producing H_2O as a coproduct.[51] The necessity of an additional electrochemical driving force to enhance the catalytic response in a similar manner has been previously observed in other molecular electrocatalysts for CO_2 reduction.[13,52] It is also noteworthy that a Ru^{II}(EDTA) complex has even been shown to convert HCO_2^- and HCO_2H to CO.[53]

A mechanism for the Ru-catalyzed dehydration reaction of HCO_2H has not yet been proposed. Previous reports have shown that a carboxylate ester of an analogous compound, $Ru^{II}(bpy)(\eta^1\text{-C(O)OCH}_2\text{CH}_2\text{OH})(CO)_2Cl$, could be converted to $[Ru^{II}(bpy)(CO)_3Cl]^+$ in the presence of HCl.[36] A carboxylate intermediate would be consistent with other observations and proposed mechanisms involving Ru(bpy) complexes, although a Ru-$[\eta^1\text{-C(O)OH}]$ species is not observed here experimentally.[20,27,54,55] Although many mechanisms could allow for this, we favor the one proposed below for the conversion of the HCO_2^- adduct to CO (Scheme 3).

The O-bound HCO_2^- species ***vi*** is capable of a hydride elimination reaction, to yield a Ru hydride with a $[CO_2]$ molecule in close proximity, ***vii***. A concomitant LMCT generates a Ru^I metal center that can immediately reduce CO_2 to form a hydroxycarbonyl species, ***viii***. Species ***viii*** is expected to be weakly hydridic as a result of the Ru^{III} oxidation state. It is therefore likely for a proton shift to occur, especially when considering the expected basicity of the bound hydroxycarbonyl. Such a protonation reaction would generate

DOI: 10.1021/jacs.5b03913
J. Am. Chem. Soc. 2015, 137, 8564−8571

Scheme 3. Proposed Dehydration Mechanism for Production of CO from HCO_2^- by 3

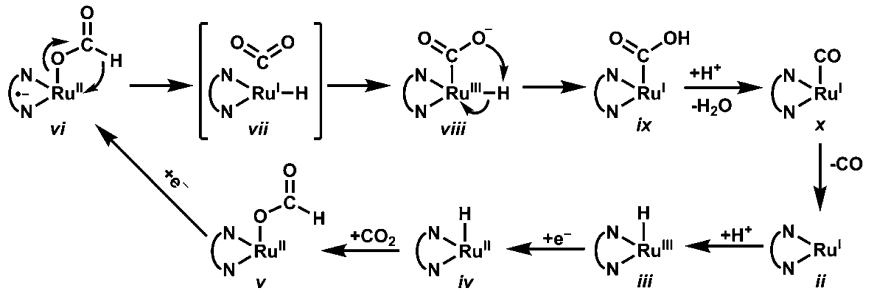

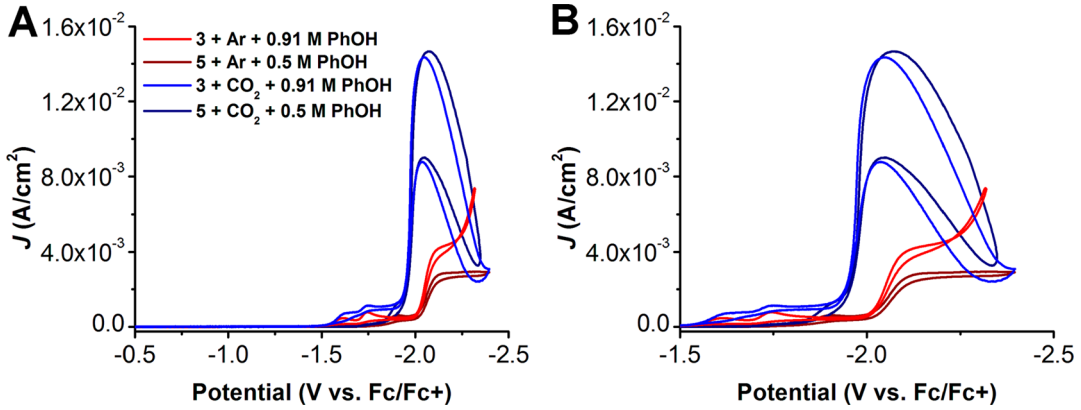

Figure 5. Cyclic voltammograms of **3** and **5** under Ar saturation (red, maroon) and CO_2 saturation (blue, navy) with added PhOH (0.91 M, red/blue; 0.5 M, maroon/red). (A) Current response and detail (B) at negative potentials. Conditions: 1 mM **3** or **5**; 0.1 M $TBAPF_6$/MeCN; glassy carbon working electrode, Pt counter electrode, Ag/AgCl pseudoreference electrode; referenced to internal ferrocene standard; scan rate 100 mV/s.

a Ru^I−[η^1-C(O)OH] species, ***ix***, which would favor protonation by an external acid to cleave the C−O bond and lose H_2O. As an octahedral 19-electron complex the resulting Ru^I species, ***x***, should rapidly lose CO. The loss of CO as an axial ligand would regenerate ***ii***, which is the entry point to the catalytic cycle that was discussed in Scheme 2. Consecutive protonation and reduction steps will generate a hydride, which can undergo a CO_2 insertion reaction to generate Ru^{II}-(η^1-OCHO) again.

To test certain elements of this proposed mechanism, a series of experiments were performed with HCO_2H and tetraethylammonium formate ($TEA^+[HCO_2^-]$).[56] Bulk electrolysis experiments at ∼−2.2 V vs Fc/Fc+ with **3** and an excess of either HCO_2H or $TEA[HCO_2^-]$ showed that CO was produced in both circumstances.[53,57] Heating complex **3** to reflux in MeCN with $TEA^+[HCO_2^-]$ under a static N_2 blanket with a gas bubbler attached via tubing to a reflux condenser allowed us to confirm by GC that CO was produced under these conditions as well as CO_2 and H_2. Any attempts to abstract or displace a chloride with a HCO_2^- salt resulted in similar behavior. Interestingly, the preparation of a partially chloride-abstracted species with trifluoromethanesulfonic acid (HOTf), Ru^{II}(mesbpy)$(CO)_2$[OTf]Cl, **4**, did not allow for the isolation of a stable formato species. Electrochemical characterization of the directly synthesized presumptive Ru−H intermediate, Ru^{II}(mesbpy)$(CO)_2$(H)Cl **5**, by CV was also consistent with the proposed mechanism. Under Ar saturation a single irreversible wave was observed at −1.98 V vs Fc/Fc+ (Figures S20 and S21). Similar to the observed behavior of **3** in the presence of a fixed concentration of PhOH, an increased current response consistent with catalysis is observed under CO_2 saturation at potentials ∼100 mV more positive than Ar saturation for **5** (Figures 5 and S21). Additionally, the voltages at peak current under CO_2 saturation (E_p = −2.07 V vs Fc/Fc+) and Ar saturation (E_p = −2.14 V vs Fc/Fc+) for **5** are also comparable to those observed for **3** (Figure 5).

Based on these experimental results, we note several key points about the observed behavior. Because of the thermodynamic considerations and factors that relate the production of CO and HCO_2H from CO_2, it is remarkable that such a delicate balance can be achieved in this system. It is possible to rationalize this by considering the equilibrium that relates CO and HCO_2H. The common intermediate shared by CO_2 and the potential products (CO, HCO_2H) in this system is a Ru−H species. In the absence of applied potential, the Ru^{II} metal center decomposes HCO_2^- and HCO_2H to CO_2 and H_2, which suggests that the Ru^{II}−H is less hydridic than HCO_2H or HCO_2^-. Under electrochemical conditions, intermediate applied potential is enough to disrupt this equilibrium, favoring the production of HCO_2H and HCO_2^- from CO_2 by increasing the relative hydricity of the Ru−H species. At high applied potential, the observed rate of catalysis increases, which is consistent with the expected increase in the hydricity of the Ru−H. At these potentials it also appears that this reduced Ru species is capable of reacting directly with CO_2 through hydride elimination from HCO_2^-/HCO_2H. Further study is in order to increase our understanding of the branching ratio between CO and HCO_2H.

■ CONCLUSION

Mechanistic electrochemical and spectroelectrochemical studies, supplemented by the synthesis of relevant intermediates, indicate that this catalytic behavior is the result of the cooperative redox response of the bpy ligand and Ru metal

DOI: 10.1021/jacs.5b03913
J. Am. Chem. Soc. 2015, 137, 8564−8571

center at negative potentials, as well as the inhibition of Ru−Ru bond formation through sterics.[13,20] In this system CO_2 binding is the result of an insertion reaction, preceded by Ru−H bond formation, which is observed by IR-SEC. The resulting species is likely similar to $Ru^{II}(mesbpy)(\eta^1\text{-}OCOH)(CO)_2Cl$. In similar Ru systems where more than one hydride is available, high pressure is used, or relevant substrate molecules are added, HCO_2^- is observed from this insertion product.[58−64] In this case, however, an additional reduction reaction seems to accelerate a thermal process: the dehydration of HCO_2^- in the presence of H^+ to CO and H_2O. The results of these two studies suggest that the equilibria relating HCO_2H, CO_2, and H_2, and CO and H_2O can have significant consequences on the catalytic functionalization of CO_2 under electrochemical conditions. We are currently exploring additional modifications of the overall ligand structure and primary coordination sphere of the Ru metal center to further investigate this behavior.

EXPERIMENTAL SECTION

General. ^{1}H NMR spectra were recorded on a Varian 400 or Jeol 500 MHz spectrometer at 298 K and referenced to residual solvent shifts. Data manipulations were completed using *ACD*. Infrared spectra were taken on a Thermo Scientific Nicolet 6700 or a Bruker Equinox 55 spectrometer. Microanalyses were performed by Midwest Microlab for C, H, and N.

Solvents and Chemicals. All solvents were obtained from Fisher Scientific. All solvents were dried in house by storing in a moisture-free environment and dried on a custom drying system running through two alumina columns under an argon atmosphere prior to use. All compounds were obtained from Fisher Scientific, Alfa Aesar, or Sigma-Aldrich and used as obtained unless otherwise specified. Tetrabutylammonium hexafluorophosphate ($TBAPF_6$, Aldrich, 98%) was recrystallized from CH_3OH twice and dried at 90 °C overnight before use in electrochemistry.

Synthetic Methods. The ligand 6,6′-dimesityl-2,2′-bipyridine, tetraethylammonium formate, and $[Ru(CO)_2Cl_2]$ were prepared according to literature methods.[13,20−22,56]

*trans-Cl-Ru(6,6′-dimesityl-2,2′-bipyridyl)(CO)$_2$Cl$_2$, **3**.* A round-bottom flask was charged with $[Ru(CO)_2Cl_2]_n$ (0.288 g, 1.26 mmol) and 6,6′-dimesityl-2,2′-bipyridine (0.500 g, 1.26 mmol) in dry toluene (25 mL). A reflux condenser was attached to the flask, and the mixture was heated to reflux and left overnight (18 h) in the dark. After this time the solution was allowed to cool to room temperature and placed in a freezer at −20 °C for 1 h. Over the course of 1 h, a pale yellow powder precipitated, which was isolated by vacuum filtration and washed with pentanes (2 × 10 mL). Yield (recovered) 580 mg, 74%. Removing the solvent from the filtrate under reduced pressure isolated a pale yellow solid from which further material could be obtained by recrystallization from THF solution with pentanes. ^{1}H NMR (d_2-CD_2Cl_2, 400 MHz): δ 8.32 (d, 2H, Ar*H*), 8.13 (d-d, 2H, Ar*H*), 7.45 (d, 2H, Ar*H*), 6.98 (s, 4H, Ar*H*), 2.34 (s, 6H, −C*H*$_3$), 2.14 (s, 12H, −C*H*$_3$). ^{13}C{^{1}H} NMR (d_2-CD_2Cl_2, 500 MHz): δ 191.26, 165.19, 157.98, 141.38, 140.21, 139.75, 138.09, 130.40, 129.58, 129.39, 123.51, 115.96, 21.96, 21.74. IR (CH_2Cl_2) ν_{CO}: 2062, 1999 cm^{-1}. ESI-MS (*m*/*z*) [M + Na$^+$]$^+$: Calcd 643.05. Found: 643.17. Elemental Analysis for $C_{30}H_{28}Cl_2N_2O_2Ru$ Calcd: C, 58.04; H, 4.55; N, 4.51. Found: C, 58.21; H, 4.60; N, 4.32.

*Ru(6,6′-dimesityl-2,2′-bipyridyl)(CO)$_2$(CF$_3$SO$_3$)Cl, **4**.* A Schlenk flask was charged with **4** (0.100 g, 0.16 mmol) in dry CH_2Cl_2 (2 mL) under a N_2 atmosphere. An excess of trifluoromethanesulfonic acid (0.30 mL, 3.2 mmol) was added slowly via syringe. The mixture was stirred for 1 h in the dark under a N_2 atmosphere. After this time diethyl ether (20 mL) was added to the solution and a white precipitate formed which was collected by filtration. Yield (recovered) 84 mg, 61%. ^{1}H NMR (d_2-CD_2Cl_2, 400 MHz): δ 8.69 (br m, 2H, Ar*H*), 8.58 (br m, 2H, Ar*H*), 7.95 (br m, 2H, Ar*H*), 7.05 (s, 4H, Ar*H*), 2.36 (s, 6H, −C*H*$_3$), 2.12 (s, 12H, −C*H*$_3$). IR (CH_2Cl_2) ν_{CO}: 2086, 2014 cm^{-1}. Elemental Analysis for $C_{31}H_{28}ClF_3N_2O_5RuS$ Calcd: C, 50.72; H, 3.84; N, 3.82. Found: C, 50.38; H, 4.34; N, 3.84.

Ru(6,6′-dimesityl-2,2′-bipyridyl)(CO)$_2$(COOMe)Cl. A round-bottom flask was charged with **mesbpy** (0.193 g, 0.49 mmol) and a dichlorotricarbonylruthenium(II) dimer (0.125 g, 0.24 mmol) in dry methyl formate (10 mL) under a N_2 atmosphere. The mixture was stirred at reflux for 2 h in the dark. After this time the solution was condensed under reduced pressure and recrystallized from a mixture of CH_2Cl_2 and pentanes. Yield (recovered) 163 mg, 52%. ^{1}H NMR (d_2-CD_2Cl_2, 400 MHz): δ 8.68 (br m, 2H, Ar*H*), 8.32 (br m, 2H, Ar*H*), 7.53 (br m, 2H, Ar*H*), 6.99 (s, 4H, Ar*H*), 3.10 (s, 3H, −C*H*$_3$), 2.34 (s, 6H, −C*H*$_3$), 2.06 (s, 12H, −C*H*$_3$). ^{13}C{^{1}H} NMR (d_2-CD_2Cl_2, 500 MHz): δ 189.07, 186.65, 185.04, 177.67, 177.55, 177.30, 158.36, 145.52, 136.72, 129.53, 123.57, 121.34, 115.98, 21.67, 20.84. IR (CH_2Cl_2) ν_{CO}: 2134, 2127, and 2059 cm^{-1}; ν_{OCO} 1611, 1606 cm^{-1}. ESI-MS (*m*/*z*) [M−Cl]$^+$: Calcd 609.13. Found: 609.26. Elemental Analysis for $C_{32}H_{31}ClN_2O_4Ru{\cdot}0.5\ CH_2Cl_2$ Calcd: C, 56.85; H, 4.70; N, 4.08. Found: C, 56.54; H, 4.45; N, 4.14.

*Ru(6,6′-dimesityl-2,2′-bipyridyl)(CO)$_2$(H)Cl, **5**.* A round-bottom flask was charged with **mesbpy** (0.193 g, 0.49 mmol) and a dichlorotricarbonylruthenium(II) dimer (0.250 g, 0.49 mmol) in dry methyl formate (10 mL) under a N_2 atmosphere. The mixture was stirred at reflux for 30 min in the dark. After this time the solution was condensed under reduced pressure and loaded onto neutral alumina with CH_2Cl_2. Running a column on silica gel with ethyl acetate (100%) recovered a single fraction containing the **mesbpy** ligand. Switching to CH_2Cl_2 as the eluent with a MeOH gradient (0 to 10%) recovered a single fraction, which was condensed under reduced pressure and found to contain **Ru(mesbpy)(CO)$_2$(H)Cl** as a tan powder. Yield (recovered) 75 mg, 26%. ^{1}H NMR (d_2-CD_2Cl_2, 500 MHz): δ 8.27 (m, 2H, Ar*H*), 8.10 (m, 2H, Ar*H*), 7.44 (m, 2H, Ar*H*), 6.97 (m, 4H, Ar*H*), 2.33 (d, 6H, −C*H*$_3$), 2.18 (d, 6H, −C*H*$_3$), 1.94 (d, 6H, −C*H*$_3$), −11.69 (s, 1H, Ru−H). ^{13}C{^{1}H} NMR (d_2-CD_2Cl_2, 500 MHz): δ 198.14, 196.55, 165.22, 163.55, 158.53, 156.81, 141.44, 140.06, 139.81, 139.59, 139.44, 137.28, 136.98, 135.71, 135.13, 129.20, 128.83, 128.47, 127.91, 127.84, 122.41, 122.32, 21.84, 21.54, 20.81, 20.53. IR (CH_2Cl_2) ν_{CO}: 2032, 1951 cm^{-1}. ESI-MS (*m*/*z*) [M−Cl]$^+$: Calcd 551.13. Found: 551.19. Elemental Analysis for $C_{30}H_{29}ClN_2O_4Ru$ Calcd: C, 61.48; H, 4.99; N, 4.78. Found: C, 61.18; H, 4.91; N, 4.63.

Electrochemistry. Electrochemical experiments were carried out using a BAS Epsilon potentiostat. For all experiments, a single compartment cell was used with a dry stir bar and a dry needle was connected to control the atmosphere. A 3 mm diameter glassy carbon electrode from BASi was employed as the working electrode. The counter electrode was a platinum (Pt) wire, and the pseudoreference electrode was a silver/silver chloride (Ag/AgCl) electrode separated from solution by a Vycor tip. Experiments were run with and without an added internal reference of ferrocene. All solutions were in dry MeCN and contained 1 mM of catalyst and 0.1 M tetrabutylammonium hexafluorophosphate ($TBAPF_6$) as the supporting electrolyte, unless otherwise noted. Scan rates were 100 mV/s unless otherwise indicated. Experiments were purged with N_2 or CO_2 (to saturation at 0.28 M) before CVs were taken and stirred in between successive experiments. All experiments reported referenced an internal ferrocene standard except for the bulk electrolysis experiments, which used the pseudoreference electrode Ag/AgCl behind a Vycor tip.

Infrared Spectroelectrochemistry. The experimental setup and design of the IR-SEC cell has been published previously by our lab.[33,34] A Pine Instrument Company model AFCBP1 bipotentiostat was employed. As the potential was scanned, thin layer bulk electrolysis was monitored by Fourier-Transform Reflectance IR off the electrode surface. All experiments were conducted in 0.1 M $TBAPF_6$/MeCN solutions with catalyst concentrations of ∼5 mM (unless otherwise noted) prepared under a nitrogen atmosphere. For IR-SEC experiments under catalytic conditions, air-free samples were sparged briefly with $^{12}CO_2$ (10−20 s). The IR-SEC cells used (working electrode/counter electrode/reference electrode) were either glassy carbon/Ag/Pt or Pt/Ag/Pt, meaning that all potentials were in

DOI: 10.1021/jacs.5b03913
J. Am. Chem. Soc. 2015, 137, 8564−8571

reference to a pseudoreference electrode, Ag/Ag+ (~+200 mV from the Fc/Fc+ couple).

X-ray Crystallography. Single crystal X-ray diffraction studies reported herein were carried out on a Bruker Kappa APEX-II CCS diffractometer equipped with Mo Kα radiation (λ = 0.71073 Å). The crystals were mounted on a Cryoloop while in Paratone oil. The data were collected under a stream of N_2 gas at 100(2) K using ω and ϕ scans. Data were integrated using the Bruker SAINT software program and scaled using SADABS software. A complete phasing model consistent with the molecular structure was produced by SHELXS direct methods. Non-hydrogen atoms were refined anisotropically by full matrix least-squares (SHELXL-97).[65] All hydrogen atoms were determined using a riding model with positions constrained to their parent atom using the appropriate FHIX command. Crystallographic data are in the Supporting Information (Table S1).

Calculations. Complexes were geometry-optimized using the BP86 functional with TZ2P basis sets. The resulting structures were confirmed as minima through analytical frequency calculations at the same level of theory. Kohn−Sham orbital representations were generated using the ADF GUI. All calculations were performed with the ADF 2012.01 software suite in collaboration with the research group of Prof. Joshua S. Figueroa.

■ ASSOCIATED CONTENT

Supporting Information

A selection of cyclic voltammograms, X-ray crystallographic information tables, IR-SEC plots, and chemical reductions. The Supporting Information is available free of charge on the ACS Publications website at DOI: 10.1021/jacs.5b03913.

■ AUTHOR INFORMATION

Corresponding Author

*ckubiak@ucsd.edu

Notes

The authors declare no competing financial interest.

■ ACKNOWLEDGMENTS

We acknowledge support for this work from the AFOSR through a Basic Research Initiative (BRI) grant (FA9550-12-1-0414) and the UCSD Department of Chemistry and Biochemistry for analytical instrumentation. We also acknowledge the assistance of Dr. Curtis Moore in obtaining and solving the molecular structure presented here through single crystal X-ray diffraction studies. We acknowledge the UCSD Chemistry and Biochemistry Molecular MS facility for use of their facilities and Steven A. Chabolla for his assistance with ESI-MS. All calculations were performed in collaboration with Prof. Joshua S. Figueroa.

■ REFERENCES

(1) Benson, E. E.; Kubiak, C. P.; Sathrum, A. J.; Smieja, J. M. *Chem. Soc. Rev.* **2009**, *38*, 89.

(2) Finn, C.; Schnittger, S.; Yellowlees, L. J.; Love, J. B. *Chem. Commun.* **2012**, *48*, 1392.

(3) Inglis, J. L.; MacLean, B. J.; Pryce, M. T.; Vos, J. G. *Coord. Chem. Rev.* **2012**, *256*, 2571.

(4) Grice, K. A.; Kubiak, C. P. In *Advances in Inorganic Chemistry*; Aresta, M., van Eldik, R., Eds.; Academic Press: San Diego, USA, 2014.

(5) Qiao, J.; Liu, Y.; Hong, F.; Zhang, J. *Chem. Soc. Rev.* **2014**, *43*, 631.

(6) Appel, A. M.; Bercaw, J. E.; Bocarsly, A. B.; Dobbek, H.; DuBois, D. L.; Dupuis, M.; Ferry, J. G.; Fujita, E.; Hille, R.; Kenis, P. J. A.; Kerfeld, C. A.; Morris, R. H.; Peden, C. H. F.; Portis, A. R.; Ragsdale, S. W.; Rauchfuss, T. B.; Reek, J. N. H.; Seefeldt, L. C.; Thauer, R. K.; Waldrop, G. L. *Chem. Rev.* **2013**, *113*, 6621.

(7) Costentin, C.; Passard, G.; Robert, M.; Savéant, J.-M. *Proc. Natl. Acad. Sci. U.S.A.* **2014**, *111*, 14990.

(8) Costentin, C.; Savéant, J.-M. *ChemElectroChem.* **2014**, *1*, 1226.

(9) Costentin, C.; Passard, G.; Savéant, J.-M. *J. Am. Chem. Soc.* **2015**, *137*, 5461.

(10) Costentin, C.; Robert, M.; Saveant, J.-M. *Chem. Soc. Rev.* **2013**, *42*, 2423.

(11) Costentin, C.; Drouet, S.; Robert, M.; Savéant, J.-M. *Science* **2012**, *338*, 90.

(12) Froehlich, J. D.; Kubiak, C. P. *J. Am. Chem. Soc.* **2015**, *137*, 3565.

(13) Sampson, M. D.; Nguyen, A. D.; Grice, K. A.; Moore, C. E.; Rheingold, A. L.; Kubiak, C. P. *J. Am. Chem. Soc.* **2014**, *136*, 5460.

(14) Smieja, J. M.; Benson, E. E.; Kumar, B.; Grice, K. A.; Seu, C. S.; Miller, A. J. M.; Mayer, J. M.; Kubiak, C. P. *Proc. Natl. Acad. Sci. U.S.A.* **2012**, *109*, 15646.

(15) Savéant, J.-M. *Chem. Rev.* **2008**, *108*, 2348.

(16) Ishida, H.; Fujiki, K.; Ohba, T.; Ohkubo, K.; Tanaka, K.; Terada, T.; Tanaka, T. *J. Chem. Soc., Dalton Trans.* **1990**, 2155.

(17) Chardon-Noblat, S.; Deronzier, A.; Ziessel, R.; Zsoldos, D. *Inorg. Chem.* **1997**, *36*, 5384.

(18) Collomb-Dunand-Sauthier, M.-N.; Deronzier, A.; Ziessel, R. *Inorg. Chem.* **1994**, *33*, 2961.

(19) Chardon-Noblat, S.; Cripps, G. H.; Deronzier, A.; Field, J. S.; Gouws, S.; Haines, R. J.; Southway, F. *Organometallics* **2001**, *20*, 1668.

(20) Kuramochi, Y.; Itabashi, J.; Fukaya, K.; Enomoto, A.; Yoshida, M.; Ishida, H. *Chem. Sci.* **2015**, *6*, 3063.

(21) Schmittel, M.; Ganz, A.; Schenk, W. A.; Hagel, M. *Z. Naturforsch.* **1999**, *54b*, 559.

(22) Cleare, M. J.; Griffith, W. P. *J. Chem. Soc. A* **1969**, 372.

(23) Gagne, R. R.; Allison, J. L.; Ingle, D. M. *Inorg. Chem.* **1979**, *18*, 2767.

(24) Gagne, R. R.; Ingle, D. M. *J. Am. Chem. Soc.* **1980**, *102*, 1444.

(25) Fujita, E.; Creutz, C.; Sutin, N.; Szalda, D. J. *J. Am. Chem. Soc.* **1991**, *113*, 343.

(26) McCarthy, B. D.; Martin, D. J.; Rountree, E. S.; Ullman, A. C.; Dempsey, J. L. *Inorg. Chem.* **2014**, *53*, 8350.

(27) Chardon-Noblat, S.; Deronzier, A.; Ziessel, R.; Zsoldos, D. *J. Electroanal. Chem.* **1998**, *444*, 253.

(28) Horvath, S.; Fernandez, L. E.; Appel, A. M.; Hammes-Schiffer, S. *Inorg. Chem.* **2013**, *52*, 3643.

(29) Raamat, E.; Kaupmees, K.; Ovsjannikov, G.; Trummal, A.; Kütt, A.; Saame, J.; Koppel, I.; Kaljurand, I.; Lipping, L.; Rodima, T.; Pihl, V.; Koppel, I. A.; Leito, I. *J. Phys. Org. Chem.* **2013**, *26*, 162.

(30) Solis, B. H.; Hammes-Schiffer, S. *Inorg. Chem.* **2014**, *53*, 6427.

(31) Whittlesey, M. K.; Perutz, R. N.; Moore, M. H. *Organometallics* **1996**, *15*, 5166.

(32) Salsman, J. C.; Kubiak, C. P. In *Spectroelectrochemistry*; Kaim, W., Klein, A., Eds.; Royal Society of Chemistry: Cambridge, U.K., 2008.

(33) Machan, C. W.; Sampson, M. D.; Chabolla, S. A.; Dang, T.; Kubiak, C. P. *Organometallics* **2014**, *33*, 4550.

(34) Zavarine, I. S.; Kubiak, C. P. *J. Electroanal. Chem.* **2001**, *495*, 106.

(35) Haukka, M.; Kiviaho, J.; Ahlgren, M.; Pakkanen, T. A. *Organometallics* **1995**, *14*, 825.

(36) Haukka, M.; Hirva, P.; Luukkanen, S.; Kallinen, M.; Ahlgrén, M.; Pakkanen, T. A. *Inorg. Chem.* **1999**, *38*, 3182.

(37) Eskelinen, E.; Haukka, M.; Venäläinen, T.; Pakkanen, T. A.; Wasberg, M.; Chardon-Noblat, S.; Deronzier, A. *Organometallics* **2000**, *19*, 163.

(38) Luukkanen, S.; Homanen, P.; Haukka, M.; Pakkanen, T. A.; Deronzier, A.; Chardon-Noblat, S.; Zsoldos, D.; Ziessel, R. *Appl. Catal., A* **1999**, *185*, 157.

(39) Gibson, D. H. *Coord. Chem. Rev.* **1999**, *185−186*, 335.

(40) Gibson, D. H.; Ding, Y.; Miller, R. L.; Sleadd, B. A.; Mashuta, M. S.; Richardson, J. F. *Polyhedron* **1999**, *18*, 1189.

(41) Sampson, M. D.; Froehlich, J. D.; Smieja, J. M.; Benson, E. E.; Sharp, I. D.; Kubiak, C. P. *Energy Environ. Sci.* **2013**, *6*, 3748.

(42) Darensbourg, D. J.; Rokicki, A.; Darensbourg, M. Y. *J. Am. Chem. Soc.* **1981**, *103*, 3223.

DOI: 10.1021/jacs.5b03913
J. Am. Chem. Soc. 2015, 137, 8564−8571

(43) Sullivan, B. P.; Meyer, T. J. *Organometallics* **1986**, *5*, 1500.
(44) Lehn, J.-M.; Ziessel, R. *J. Organomet. Chem.* **1990**, *382*, 157.
(45) Sahara, G.; Ishitani, O. *Inorg. Chem.* **2015**, *54*, 5096.
(46) Sekizawa, K.; Maeda, K.; Domen, K.; Koike, K.; Ishitani, O. *J. Am. Chem. Soc.* **2013**, *135*, 4596.
(47) Sun, D.; Gao, Y.; Fu, J.; Zeng, X.; Chen, Z.; Li, Z. *Chem. Commun.* **2015**, *51*, 2645.
(48) Coffey, R. S. *Chem. Commun.* **1967**, 923b.
(49) Halpern, J.; Kemp, A. L. W. *J. Am. Chem. Soc.* **1966**, *88*, 5147.
(50) Anderson, P. A.; Deacon, G. B.; Haarmann, K. H.; Keene, F. R.; Meyer, T. J.; Reitsma, D. A.; Skelton, B. W.; Strouse, G. F.; Thomas, N. C. *Inorg. Chem.* **1995**, *34*, 6145.
(51) Matubayasi, N.; Nakahara, M. *J. Chem. Phys.* **2005**, *122*, 074509.
(52) Riplinger, C.; Sampson, M. D.; Ritzmann, A. M.; Kubiak, C. P.; Carter, E. A. *J. Am. Chem. Soc.* **2014**, *136*, 16285.
(53) Shimizu, K. *Bull. Chem. Soc. Jpn.* **1977**, *50*, 2921.
(54) Voyame, P.; Toghill, K. E.; Méndez, M. A.; Girault, H. H. *Inorg. Chem.* **2013**, *52*, 10949.
(55) Coalter, J. N.; Huffman, J. C.; Caulton, K. G. *Organometallics* **2000**, *19*, 3569.
(56) Grills, D. C.; Farrington, J. A.; Layne, B. H.; Lymar, S. V.; Mello, B. A.; Preses, J. M.; Wishart, J. F. *J. Am. Chem. Soc.* **2014**, *136*, 5563.
(57) Fenwick, A. Q.; Luca, O. R. *J. Photochem. Photobiol. B*, DOI: 10.1016/j.jphotobiol.2015.04.003.
(58) Musashi, Y.; Sakaki, S. *J. Am. Chem. Soc.* **2000**, *122*, 3867.
(59) Komiya, S.; Yamamoto, A. *J. Organomet. Chem.* **1972**, *46*, C58.
(60) Kolomnikov, I. S.; Gusev, A. I.; Aleksandrov, G. G.; Lobeeva, T. S.; Struchkov, Y. T.; Vol'pin, M. E. *J. Organomet. Chem.* **1973**, *59*, 349.
(61) Jessop, P. G.; Ikariya, T.; Noyori, R. *Nature* **1994**, *368*, 231.
(62) Munshi, P.; Main, A. D.; Linehan, J. C.; Tai, C.-C.; Jessop, P. G. *J. Am. Chem. Soc.* **2002**, *124*, 7963.
(63) Urakawa, A.; Jutz, F.; Laurenczy, G.; Baiker, A. *Chem.—Eur. J.* **2007**, *13*, 3886.
(64) Jessop, P. G.; Hsiao, Y.; Ikariya, T.; Noyori, R. *J. Am. Chem. Soc.* **1996**, *118*, 344.
(65) Sheldrick, G. *Acta Crystallogr. A* **2008**, *64*, 112.

DOI: 10.1021/jacs.5b03913
J. Am. Chem. Soc. 2015, 137, 8564−8571